

Electromagnetic evanescent field associated with surface acoustic wave:

Response of metallic thin films

Takuya Kawada,^{1,2,*} Kei Yamamoto,^{3,4,†} Masashi Kawaguchi,¹ Hiroki Matsumoto,^{1,5} Ryusuke Hisatomi,^{5,6} Hiroshi Kohno,⁷ Sadamichi Maekawa,^{3,4,8} and Masamitsu Hayashi^{9,10}

¹*Department of Physics, The University of Tokyo, Bunkyo, Tokyo 113-0033, Japan*

²*Department of Basic Science, The University of Tokyo, Bunkyo, Tokyo 113-0033, Japan*

³*Advanced Science Research Center,
Japan Atomic Energy Agency, Tokai, Ibaraki 319-1195, Japan*

⁴*RIKEN Center for Emergent Matter Science, Wako, Saitama 351-0198, Japan*

⁵*Institute for Chemical Research, Kyoto University, Uji, Kyoto 611-0011, Japan*

⁶*Center for Spintronics Research Network (CSRN),
Kyoto University, Uji, Kyoto 611-0011, Japan*

⁷*Department of Physics, Nagoya University, Chikusa, Nagoya 464-8602, Japan*

⁸*Kavli Institute for Theoretical Sciences,
University of Chinese Academy of Sciences,
Beijing 100049, People's Republic of China*

⁹*Department of Physics, The University of Tokyo, Tokyo 113-0033, Japan*

¹⁰*Trans-Scale Quantum Science Institute (TSQS),
The University of Tokyo, Bunkyo, Tokyo 113-0033, Japan*

(Dated: December 20, 2024)

Abstract

Surface acoustic waves (SAWs), coherent vibrational modes localized at solid surfaces, have been employed to manipulate and detect electronic and magnetic states in condensed-matter systems via strain. SAWs are commonly excited in a piezoelectric material, often the substrate. In such systems, SAWs not only generate strain but also electric field at the surface. Conventional analysis of the electric field accompanying the SAW invokes the electrostatic approximation, which may fall short in fully capturing its essential characteristics by neglecting the effect of the magnetic field. Here we study the electric and magnetic fields associated with SAWs without introducing the electrostatic approximation. The plane wave solution takes the form of an evanescent field that decays along the surface normal with a phase velocity equal to the speed of sound. If a metallic film is placed on the piezoelectric substrate, a time- and space-varying electric field permeates into the film with a decay length along the film normal defined by the skin depth and the SAW wavelength. For films with high conductivity, the phase of the electric field varies along the film normal. The emergence of the evanescent field is a direct consequence of dropping the electrostatic approximation, providing a simple but critical physical interpretation of the SAW-induced electromagnetic field.

I. INTRODUCTION

Surface acoustic waves (SAWs), which are vibrational modes localized at the surfaces of solids, serve as distinctive tools for non-invasive manipulation and detection of the electronic states in condensed matter systems. Coherent excitation of SAWs is typically achieved by applying an rf signal to periodically spaced electrodes patterned on a piezoelectric substrate [1], which induces an accompanying ac electric field. This electric field mobilizes charge carriers within a conducting material positioned along the SAW's delay line, while the back reaction alters the SAW's amplitude and velocity [2–5]. Consequently, SAWs can be effectively employed as a contactless electrical probe operating in the microwave frequency range, offering a robust technique for tracking low-frequency conductivity [6–11] and diagnosing quantum Hall states [12–15]. In addition, the SAW has attracted a growing interest in the field of

* takuyakawada@g.ecc.u-tokyo.ac.jp

† yamamoto.kei@jaea.go.jp

spintronics as a source of rf mechanical motions that can interact with electron spins via magnetostriction [16–19], or spin-vorticity coupling [20–22]. Precise understanding of the SAW-induced electric field is thus of vital importance to distinguish electrical origins of the charge and spin dynamics from mechanical ones.

Conventional analysis of the electric field (\mathbf{E}) typically employs the electrostatic approximation [3, 23–26], which introduces a scalar potential ϕ and sets $\mathbf{E} = -\nabla\phi$. It also implies the absence of the time derivative of the magnetic field, being equivalent to neglecting the Ampère-Maxwell law. With regard to the analysis of SAW-induced electric fields, the approximation typically provides a quantitatively accurate description so far as the field amplitude is concerned since the phase velocity of the SAW (v) is about five orders of magnitude smaller than the speed of light (c). However, it may be inadequate for fully capturing characteristics of the electric field, particularly in systems involving metallic films on piezoelectric substrates. First, the approximation can yield quantitatively different conclusions if additional small parameters, comparable to v/c , are present in the system. Such parameters in the piezoelectric substrate/metal composite include the ratio of the Thomas-Fermi length ($\lambda_{\text{TF}} \sim 0.1$ nm) to the SAW wavelength ($\lambda \sim 1$ -10 μm), and the ratio of displacement current to conduction current. Second, the neglectance of the electromagnetic induction can obscure the field screening mechanisms in conducting materials. The electric field associated with the SAW turns out to include a transverse component ($\nabla \cdot \mathbf{E} = 0$) and, according to the Faraday’s law, must induce an ac magnetic field. In metals, this magnetic field leads to the screening of electromagnetic waves via electric currents to satisfy the Ampère-Maxwell law, a phenomenon known as the skin effect; the penetration is characterized by the skin depth, which is typically several tens of micrometers for microwave frequency fields. Under the electrostatic approximation, however, the skin effect cannot be treated due to the absence of the magnetic field.

In this work, we study electric and magnetic fields associated with SAW without invoking the electrostatic approximation and identify the applicable conditions. We find that the SAW generates a transverse electric field, which can be considered as an electromagnetic evanescent wave that travels at the speed of sound, in addition to the conventional longitudinal electric field. We derive the decay length of the former, which is determined by the SAW wavelength and the skin depth. For films with large conductivity and thickness, the distribution of the electric field inside the film is a quantitatively different from that under

the electrostatic approximation. The electrostatic approximation is justified when the skin depth is sufficiently larger than the SAW wavelength, which is not necessarily always the case for metallic films. This work bridges the gap between the general framework for the electromagnetic response of metallic films and the simplified treatment under the electrostatic approximation commonly employed in SAW studies, offering a clear and straightforward physical interpretation of the SAW-induced electric field.

II. SETUP

We are primarily concerned with plane wave propagation along the interface between a piezoelectric substrate and a (nonmagnetic) conducting layer of thickness d facing vacuum. Let the xyz coordinate system be oriented such that the wave propagates along x and the substrate occupies $z < 0$ as shown in Fig. 1. We would like to know the electromagnetic waves described by the macroscopic Maxwell's equations,

$$\partial_t \mathbf{B} = -\nabla \times \mathbf{E}, \quad (1)$$

$$0 = \nabla \cdot \mathbf{B}, \quad (2)$$

$$\partial_t \mathbf{D} = \nabla \times \mathbf{H} - \mathbf{J}, \quad (3)$$

$$0 = \nabla \cdot \mathbf{D} - \rho, \quad (4)$$

where ρ , \mathbf{J} denote the free charge density and current density, respectively. Different material media are distinguished by the constitutive relations between \mathbf{E} , \mathbf{H} and \mathbf{D} , \mathbf{B} as well as the assumptions on the free charges. We model each region as follows:

Vacuum ($z > d$):

$$\mathbf{D} = \varepsilon_0 \mathbf{E}, \quad \mathbf{B} = \mu_0 \mathbf{H}, \quad \rho = 0, \quad \mathbf{J} = \mathbf{0}, \quad (5)$$

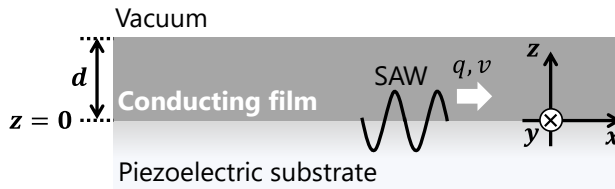


FIG. 1. Schematic illustration of the system, composed of a piezoelectric substrate ($z < 0$), a conducting slab ($0 < z < d$), and the vacuum ($z > d$). A piezoelectrically excited SAW, with wavenumber q and phase velocity v along x , travels on the surface of the substrate.

where ε_0, μ_0 are the permittivity and permeability of vacuum respectively.

Conducting slab ($0 < z < d$):

$$\begin{aligned} \mathbf{D} &= \varepsilon_r \varepsilon_0 \mathbf{E}, \quad \mathbf{B} = \mu_0 \mathbf{H}, \\ \partial_t \rho + \nabla \cdot \mathbf{J} &= 0, \quad \mathbf{J} = \sigma_c \mathbf{E} - D_e \nabla \rho, \end{aligned} \quad (6)$$

where $\varepsilon_r, \sigma_c, D_e$ are the relative permittivity, conductivity, and the diffusion constant.

Piezoelectric substrate ($z < 0$):

$$\mathbf{D} = \hat{\varepsilon} \mathbf{E} + \mathbf{P}, \quad \mathbf{B} = \mu_0 \mathbf{H}, \quad \rho = 0, \quad \mathbf{J} = \mathbf{0}, \quad (7)$$

where $\hat{\varepsilon}$ is the dielectric tensor, and $\mathbf{P} = \hat{e} \hat{\varepsilon}$ is the electric polarization associated with the linear strain tensor $\hat{\varepsilon}$ through the piezoelectric tensor \hat{e} . The displacement vector \mathbf{u} , related to the strain by $\varepsilon_{ij} = (\partial_j u_i + \partial_i u_j)/2$, obeys the equation of motion,

$$m_p \partial_t^2 u_i = c_{ijkl} \partial_j \partial_l u_k - e_{kij} \partial_j E_k, \quad (8)$$

where m_p is the mass density of the piezoelectric substrate and c_{ijkl} is the elastic stiffness tensor. Repeated Latin indices are understood to be summed over.

Since all the equations involved are linear, the solutions can be sought in the form $f(z) e^{iq(x-vt)}$ where q and v are the in-plane wavenumber and phase velocity, respectively. To avoid notational mess, we hereafter understand all the dependent variables are of this form and suppress the appearance of $e^{i(qx-\omega t)}$. Under our assumption that $\mathbf{B} = \mu_0 \mathbf{H}$ holds everywhere, we can eliminate \mathbf{B} and \mathbf{H} via Eqs. (1) and (2),

$$iqv \begin{pmatrix} B_x \\ B_y \\ B_z \end{pmatrix} = \begin{pmatrix} -\partial_z E_y \\ \partial_z E_x - iqE_z \\ iqE_y \end{pmatrix}, \quad \partial_z B_z = -iqB_x. \quad (9)$$

Note that Eq. (2) is redundant for $\omega \equiv qv \neq 0$. From Eqs. (1) and (3), one obtains

$$q^2 v^2 \mu_0 \begin{pmatrix} D_x \\ D_y \\ D_z \end{pmatrix} = \begin{pmatrix} -\partial_z^2 E_x + iq \partial_z E_z \\ (q^2 - \partial_z^2) E_y \\ iq \partial_z E_x + q^2 E_z \end{pmatrix} - iqv \mu_0 \begin{pmatrix} J_x \\ J_y \\ J_z \end{pmatrix}. \quad (10)$$

We again note that the constraint Eq. (4) becomes redundant for $\omega\rho \neq 0$ because ρ and \mathbf{J} satisfy the conservation law. The equations are supplemented by boundary conditions appropriate for different material interfaces. In the following, we first solve the equations in each region with a boundary condition if it can be discussed independently of the other regions. We then glue the solutions together at the interfaces by imposing the remaining boundary conditions.

III. SOLUTION IN EACH REGION

In this section, we solve Eq. (10) in each region separately. The obtained solutions will be conjoined by the electromagnetic boundary conditions in the next section.

A. Vacuum half-space

First we consider the vacuum half-space ($z > d$). We demonstrate that the evanescent field is a universal feature of vacuum electromagnetic waves forced to propagate slower than the speed of light c . Noting $\mu_0\varepsilon_0 = 1/c^2$, Eq. (10) yields

$$\frac{q^2 v^2}{c^2} \begin{pmatrix} E_x \\ E_y \\ E_z \end{pmatrix} = \begin{pmatrix} -\partial_z^2 E_x + iq\partial_z E_z \\ (q^2 - \partial_z^2) E_y \\ iq\partial_z E_x + q^2 E_z \end{pmatrix}. \quad (11)$$

Imposing the vanishing boundary condition at $z \rightarrow \infty$, one obtains from Eq. (11),

$$\begin{pmatrix} E_x \\ E_z \end{pmatrix} = C^{\text{TM}} \begin{pmatrix} 1 \\ i\gamma \end{pmatrix} e^{-q(z-d)/\gamma}, \quad (12)$$

$$E_y = C^{\text{TE}} e^{-q(z-d)/\gamma}, \quad (13)$$

where $\gamma = 1/\sqrt{1 - v^2/c^2}$ is the Lorentz factor, and we assume $q > 0$ in the following. The integration constants, C^{TE} and C^{TM} , will be determined by the boundary conditions at $z = d$. Equations (12) and (13) represent the transverse magnetic (TM) and the transverse electric (TE) modes, respectively.

The above solution has been derived independently of the boundary conditions at $z = d$. This shows that any electromagnetic waves in vacuum that decay at infinity ($z \rightarrow \infty$) automatically take the form of the evanescent wave [27], as pointed out for the special case

of the Bleustein-Glyaev type SAW [28, 29] in highly symmetric piezoelectric materials [30]. As an example, the TM mode Eq. (12) is schematically illustrated in Fig. 2. The electric and magnetic field lines display the presence of an electromagnetic field associated with the SAW. Note that going beyond the electrostatic approximation predicts a nonzero magnetic field, hence the transverse component of the electric field, associated with the SAW. Although the magnetic field component is significantly smaller compared to the free electromagnetic field, this result can potentially be relevant because it directly couples to electron spin and magnetization [31, 32].

B. Conducting slab

Next we consider the solution inside a conducting slab. We assume that the conductor is isotropic, and introduce the reduced speed of light $c_m = (\mu_0 \varepsilon_0 \varepsilon_r)^{-1/2}$, the skin depth $\delta_m = \sqrt{2/qv\mu_0\sigma_c}$, and the Thomas-Fermi length $\lambda_{\text{TF}} = \sqrt{D_e \varepsilon_0 \varepsilon_r / \sigma_c}$. One then obtains

$$\left(\frac{q^2 v^2}{c_m^2} + \frac{2i}{\delta_m^2} \right) \begin{pmatrix} E_x \\ E_y \\ E_z \end{pmatrix} = \begin{pmatrix} -\partial_z^2 E_x + iq\partial_z E_z \\ (q^2 - \partial_z^2) E_y \\ iq\partial_z E_x + q^2 E_z \end{pmatrix} + \frac{2i\lambda_{\text{TF}}^2}{\varepsilon_0 \varepsilon_r \delta_m^2} \begin{pmatrix} iq\rho \\ 0 \\ \partial_z \rho \end{pmatrix}, \quad (14)$$

with

$$\rho = \varepsilon_0 \varepsilon_r (iqE_x + \partial_z E_z). \quad (15)$$

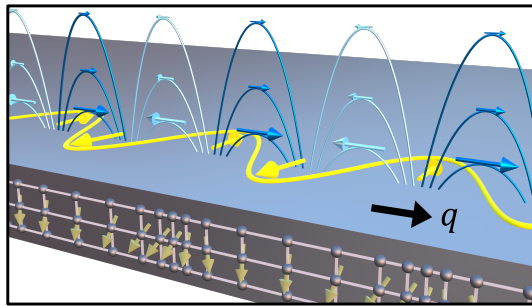


FIG. 2. Schematic illustration of the SAW-induced TM mode electromagnetic evanescent field. The purple and yellow curves with arrows represent the electric force and magnetic field, respectively. The length of the arrows indicate the strength of the corresponding fields. The green arrows show the local spontaneous polarization in the piezoelectric (e.g., LiNbO₃) substrate. The dense gray spheres represent lattice points of the substrate.

The general solutions are written in the form,

$$\mathbf{E} = \mathbf{E}^{\text{TM}} + \mathbf{E}^{\text{TE}} + \mathbf{E}^{\text{L}}, \quad (16)$$

where $\nabla \cdot \mathbf{E}^{\text{TM}} = \nabla \cdot \mathbf{E}^{\text{TE}} = 0$, $\nabla \times \mathbf{E}^{\text{L}} = 0$, and

$$\begin{aligned} \begin{pmatrix} E_x^{\text{TM}} \\ E_z^{\text{TM}} \end{pmatrix} &= C_+^{\text{TM}} \begin{pmatrix} 1 \\ -iq/\alpha \end{pmatrix} e^{\alpha(z-d)} + C_-^{\text{TM}} \begin{pmatrix} 1 \\ iq/\alpha \end{pmatrix} e^{-\alpha z}, \\ E_y^{\text{TE}} &= C_+^{\text{TE}} e^{\alpha(z-d)} + C_-^{\text{TE}} e^{-\alpha z}, \\ \begin{pmatrix} E_x^{\text{L}} \\ E_z^{\text{L}} \end{pmatrix} &= C_+^{\text{L}} \begin{pmatrix} iq/Q \\ 1 \end{pmatrix} e^{Q(z-d)} + C_-^{\text{L}} \begin{pmatrix} -iq/Q \\ 1 \end{pmatrix} e^{-Qz}, \end{aligned} \quad (17)$$

with

$$\alpha = q \sqrt{1 - \frac{v^2}{c_m^2} - \frac{2i}{(q\delta_m)^2}}, \quad (18)$$

$$Q = \frac{1}{\lambda_{\text{TF}}} \sqrt{1 + (q\lambda_{\text{TF}})^2 - i\eta}, \quad (19)$$

$$\eta = \frac{qv\varepsilon_0\varepsilon_r}{\sigma_c} = \frac{v^2}{2c_m^2} (q\delta_m)^2, \quad (20)$$

whereas the other components vanish, $E_y^{\text{TM}} = E_y^{\text{L}} = E_x^{\text{TE}} = E_z^{\text{TE}} = 0$. Thus, the electric field consists of TM, TE, and longitudinal components with two integration constants each. Note that η represents the ratio of displacement current ($\varepsilon_r\varepsilon_0\partial_t E$) to drift current ($\sigma_c E$), which is several orders of magnitude smaller than unity in metals for microwave frequency field. For later use, we give electric current density and charge density,

$$\begin{pmatrix} J_x \\ J_z \end{pmatrix} = \sigma_c \begin{pmatrix} E_x^{\text{TM}} \\ E_z^{\text{TM}} \end{pmatrix} + i\eta\sigma_c \begin{pmatrix} E_x^{\text{L}} \\ E_z^{\text{L}} \end{pmatrix}, \quad J_y = \sigma_c E_y^{\text{TE}} \quad (21)$$

$$\rho = -i\varepsilon_0\varepsilon_r \frac{Q^2}{q} \left(1 - \frac{q^2}{Q^2}\right) E_x^{\text{L}}. \quad (22)$$

Without relying on the electrostatic approximation, we have obtained the precise decay length of the transverse components, Eq. (18), which explicitly takes the skin effect into account. Equation (18) reproduces the previous result $\alpha = q$ [3] if we neglect the skin effect ($\delta_m \rightarrow \infty$) and take the limit $v/c \rightarrow 0$, whereas it reduces to the ordinary skin effect if we set $v = c_m$. Since the SAW velocity v is about five orders of magnitude smaller than the speed of light, $v/c_m \ll 1$ is always satisfied. Thus the difference between the updated α

[Eq. (18)] and the conventional one [3] comes from the imaginary term under the square root. The derived expression suggests that the contribution of the skin effect cannot be neglected when δ_m is comparable to q^{-1} and in such a case it predicts a shorter decay length than the conventional model. Such a situation occurs in materials with sufficiently large conductivity and thus the result obtained here can be important especially for metallic films.

Let us proceed to discuss the boundary conditions that can be imposed independently of the other regions. Equation (17) has six integration constants corresponding to three dynamical degrees of freedom; two for photons and another for conduction electrons. Two of the constants can be eliminated by imposing $J_z = 0$ at the boundaries, enabling one to express C_{\pm}^L in terms of C_{\pm}^{TM} ;

$$\begin{pmatrix} C_+^L \\ C_-^L \end{pmatrix} = \frac{qe^{Qd}}{2\alpha\eta \sinh Qd} \begin{pmatrix} 1 - e^{-(Q+\alpha)d} & -e^{-\alpha d} + e^{-Qd} \\ e^{-\alpha d} - e^{-Qd} & -1 + e^{-(Q+\alpha)d} \end{pmatrix} \begin{pmatrix} C_+^{\text{TM}} \\ C_-^{\text{TM}} \end{pmatrix}. \quad (23)$$

Thus the general solutions in the conducting slab have four constants to be determined by the electromagnetic boundary conditions. At this stage, one already sees that the ratio $C_{\pm}^L/C_{\pm}^{\text{TM}}$ is roughly equal to $q/\alpha\eta$. This is a robust consequence of the current conservation at the boundaries and holds irrespective of the materials outside as long as they are insulating. Then, from Eq. (21), the ratio of the in-plane current induced by the longitudinal field to that by the transverse field is $\sim (q/\alpha) \cdot (q/Q)$. As explicitly shown in Sec. VI, there typically exists a hierarchy $\eta \ll q/Q \ll \alpha/q \sim 1$, so that the in-plane current is induced mostly by the transverse field. As for the electric field [Eq. (17)], the longitudinal component dominates near the interface whereas the transverse one decays slower and becomes prominent in relative terms into the depth of the metal, which is a different behavior from the electric current. This is because the electric current contains the diffusive component induced by the charge accumulation in addition to the drift current proportional to the electric field. Note that these estimates can be easily confirmed for films of infinite thickness, where $C_+^{\text{L/TM/TE}} = 0$, and

$$\begin{pmatrix} E_x \\ E_z \end{pmatrix} \propto i\eta \begin{pmatrix} i\alpha/q \\ -1 \end{pmatrix} e^{-\alpha z} - \begin{pmatrix} iq/Q \\ -1 \end{pmatrix} e^{-Qz}, \quad E_y \propto e^{-\alpha z}, \quad (24)$$

$$\begin{pmatrix} J_x \\ J_z \end{pmatrix} \propto i\eta\sigma_c \left[\begin{pmatrix} i\alpha/q \\ -1 \end{pmatrix} e^{-\alpha z} - \begin{pmatrix} iq/Q \\ -1 \end{pmatrix} e^{-Qz} \right], \quad J_y \propto \sigma_c e^{-\alpha z}. \quad (25)$$

C. Half-infinite piezoelectric substrate

In general, the analytical solutions for this case ($z < 0$) are either unavailable or intractable mainly because the system intrinsically lacks rotational symmetry. Since our model ignores mechanical degrees of freedom in the conductor, the electromagnetic field inside the piezoelectric substrate affects the conducting slabs only via the boundary conditions, i.e., the amplitudes of the electric and magnetic fields at $z = -0$. Taking advantage of this, we merely outline the framework of the numerical calculation here, avoiding the actual evaluation of the electromagnetic field and treating their interface values as input parameters in the later analysis.

The solutions can be computed by simultaneously solving Eqs. (8) and (10) under the constraints Eqs. (4) and (7) and given boundary conditions [23–26]. Eliminating \mathbf{D} by Eq. (7), there exist six unknown functions, \mathbf{u} and \mathbf{E} , governed by the six time-evolution equations (8) and (10) with one constraint Eq. (4), implying five dynamical degrees of freedom. The equations are explicitly shown in Eq. (41) in Appendix IX A, which do not contain the second order derivative of E_z with respect to z . This makes it harder to determine the order of the equations in ∂_z , or the number of the integration constants. One may thus algebraically eliminate E_z and $\partial_z E_z$ from the seven equations (Eqs. (8), (10), and Eq. (4)) and obtain five equations of second order in ∂_z for five dependent variables (u_x, u_y, u_z, E_x , and E_y), which yields ten integration constants. The number is reduced by half by demanding either exponential decay towards $z = -\infty$ [33]. The stress-free boundary condition, i.e., the vanishment of the stress normal to the substrate surface, should be able to eliminate three of the five remaining constants, leaving two to be determined through the electromagnetic boundary conditions, which in fact encode the information of the adjoining medium, i.e., the conductor facing vacuum in our case.

IV. SOLUTIONS FOR THE FULL FILM STACK

Now we are in a position to glue the solutions obtained above together by the electromagnetic boundary conditions. To guide the calculations, we first review the structure of the present boundary value problem. Per interface, there are six boundary conditions that follow from Maxwell's equations (continuity of tangential \mathbf{E} , \mathbf{H} and normal \mathbf{D} , \mathbf{B}), only four

of which are independent. This can be understood as follows. If all the field components are independent of y , the z -components of Eqs. (1) and (3),

$$\partial_t B_z = -\partial_x E_y, \quad \partial_t D_z = \partial_x H_y - J_z, \quad (26)$$

together with the plane-wave ansatz $\partial_x \rightarrow iq$, $\partial_t \rightarrow -iqv$ and the metal-insulator boundary condition $J_z = 0$ lead to

$$E_y = vB_z, \quad H_y = -vD_z \quad (27)$$

at the boundaries. Thus, the continuity of B_z, D_z is equivalent to that of E_y, H_y , leaving four independent conditions for each boundary ($z = 0$ and $z = d$). In the present system, the eight conditions are imposed on the eight integration constants; C^{TM} and C^{TE} in vacuum, C_{\pm}^{TM} and C_{\pm}^{TE} in the conducting slab, and the remaining two in the piezoelectric substrate. As C_{\pm}^{L} have been represented by C_{\pm}^{TM} [Eq. (23)], they are not included here. Note that the SAW's phase velocity v is also a parameter that must be determined. The above conditions contain v as a parameter, and we numerically look for a value of v that satisfies all conditions. Through this process, the eight integration constants are determined up to an overall multiplicative factor representing the SAW amplitude, which should be assigned by the external force to excite the SAW, e.g. the input power to the interdigital transducer.

The above procedure allows one to obtain a numerical solution for a specific stack, provided that the material constants of the piezoelectric substrate and the film are known. To obtain an analytical expression, however, is a heavy burden due to the low crystal symmetry of the substrate. As our interest here is the general behavior of the electric current and charge in the metallic film, here we assume that the parameters associated with the substrate are given and seek to provide an explicit form for C_{\pm}^{TM} and C_{\pm}^{TE} . We therefore regard v and the amplitudes,

$$E_{x0} \equiv E_x(z \rightarrow -0), \quad E_{y0} \equiv E_y(z \rightarrow -0), \quad (28)$$

as given and fixed. E_{x0} and E_{y0} , the electric field amplitude at the film/substrate interface, are later used as units for the TM and TE mode amplitudes in the conducting slab, respectively. The two parameters are in general coupled and an additional relationship arises between E_{x0} and E_{y0} . Thus one may set either E_{x0} or E_{y0} as given and express C_{\pm}^{TM} and C_{\pm}^{TE} in units of the other. However, the analytical expression of the relation, which is obtained from the boundary condition at $z = 0$ (see Appendix, Sec. IX B), is prohibitively complicated and we proceed with two fixed constants, E_{x0} and E_{y0} .

Let us consider the boundary at $z = d$ between the vacuum and conductor. Two of the four boundary conditions can be used to eliminate $C^{\text{TE/TM}}$ and the remaining two impose conditions among C_{\pm}^{TE} and C_{\pm}^{TM} . As a result, one obtains the following two equations on $C_{\pm}^{\text{TE}}, C_{\pm}^{\text{TM}}$:

$$\frac{\gamma}{q} = -\frac{1}{\alpha} \frac{C_{+}^{\text{TE}} + C_{-}^{\text{TE}} e^{-\alpha d}}{C_{+}^{\text{TE}} - C_{-}^{\text{TE}} e^{-\alpha d}}, \quad (29)$$

$$-\frac{\varepsilon_r}{\gamma} = \frac{\alpha Q (C_{+}^{\text{TM}} + C_{-}^{\text{TM}} e^{-\alpha d}) + iq (C_{+}^{\text{L}} - C_{-}^{\text{L}} e^{-Qd})}{Q q (C_{+}^{\text{TM}} - C_{-}^{\text{TM}} e^{-\alpha d}) + i\alpha (C_{+}^{\text{L}} + C_{-}^{\text{L}} e^{-Qd})}, \quad (30)$$

where C_{\pm}^{L} can be expressed with C_{\pm}^{TM} via Eq. (23). We remark that these equations are equivalent to the continuity of surface impedances $Z^{\text{TE}} = E_y/H_x = vB_z/H_x$ and $Z^{\text{TM}} = E_x/H_y = -E_x/vD_z$ across the boundary. Equations (29) and (30), together with (23), offer four conditions among six constants $C_{\pm}^{\text{TE}}, C_{\pm}^{\text{TM}}$, and C_{\pm}^{L} , which we choose to represent through two auxiliary constants, C_0^{TE} and C_0^{TM} , as

$$C_{\pm}^{\text{TE}} = \frac{C_0^{\text{TE}}}{2} \left(\frac{\alpha\gamma}{q} \mp 1 \right) e^{\alpha(d\mp d)/2}, \quad (31)$$

$$C_{\pm}^{\text{TM}} = \frac{C_0^{\text{TM}} \alpha \eta}{2q} \left\{ \left(\varepsilon_r \frac{1 - i\eta}{\gamma} \pm \frac{i\alpha\eta}{q} \right) \sinh Qd + \frac{q}{Q} (\cosh Qd - e^{\pm\alpha d}) \right\} e^{\alpha(d\mp d)/2}, \quad (32)$$

$$C_{\pm}^{\text{L}} = \pm \frac{C_0^{\text{TM}}}{2} \left\{ \frac{i\alpha\eta}{q} (e^{\pm Qd} - \cosh \alpha d) + \left(\varepsilon_r \frac{1 - i\eta}{\gamma} \mp \frac{q}{Q} \right) \sinh \alpha d \right\} e^{Q(d\mp d)/2}. \quad (33)$$

Next we move on to the boundary at $z = 0$. Looking at Eqs. (17) and (31) - (33), the continuity of E_x, E_y at $z = 0$ is sufficient to determine C_0^{TE} and C_0^{TM} in terms of E_{x0} and E_{y0} ,

$$\begin{aligned} \frac{E_{x0}}{C_0^{\text{TM}}} &= i \left(\frac{q^2}{Q^2} - \frac{\alpha^2 \eta^2}{q^2} \right) \sinh Qd \sinh \alpha d + \frac{2\alpha\eta}{Q} (\cosh Qd \cosh \alpha d - 1) \\ &\quad + \varepsilon_r \frac{1 - i\eta}{\gamma} \left(\frac{\alpha\eta}{q} \sinh Qd \cosh \alpha d + \frac{iq}{Q} \cosh Qd \sinh \alpha d \right), \quad (34) \\ \frac{E_{y0}}{C_0^{\text{TE}}} &= \sinh \alpha d + \frac{\alpha\gamma}{q} \cosh \alpha d. \end{aligned}$$

This achieves our goal of expressing the electromagnetic field and current in the conducting slab between vacuum and substrate in terms of tangential electric fields E_{x0}, E_{y0} at the substrate/film interface. We reiterate that the remaining boundary conditions, i.e., the continuity of H_x and D_z at $z = 0$, can be used to determine v and the relative amplitude between E_{x0} and E_{y0} , though we would not carry it out here (see Appendix IX B for the detail). Instead, we employ these results to evaluate the electric current and charge distribution within a metallic film.

V. ELECTROSTATIC LIMIT

A. Definition of the electrostatic approximation

Let us discuss the relation between the results described above and those obtained from the electrostatic approximation. First, we comment on the definition of the electrostatic approximation. It is often the case that one neglects the time derivative of \mathbf{B} . Setting $\partial_t \mathbf{B} = \mathbf{0}$ in Eq. (1) leads to $\nabla \times \mathbf{E} = \mathbf{0}$, which allows one to use $\mathbf{E} = -\nabla\phi$. However, Eq. (3) does not exactly hold when $\partial_t \mathbf{B} = \mathbf{0}$: substituting $\partial_t \mathbf{B} = \mathbf{0}$ into the time derivative of Eq. (3) multiplied by μ_0 reads

$$\mu_0 \partial_t^2 \mathbf{D} + \mu_0 \partial_t \mathbf{J} = 0. \quad (35)$$

This is the requirement to justify the electrostatic approximation. When \mathbf{E}^{TM} , \mathbf{E}^{TE} and \mathbf{E}^{L} in Eq. (17) are plugged into Eq. (35), one obtains

$$-q^2 \left[\left(\frac{v}{c_m} \right)^2 + \frac{2i}{(q\delta_m)^2} \right] (\mathbf{E}^{\text{TM}} + \mathbf{E}^{\text{TE}}) = 0. \quad (36)$$

Equation (36) shows that we must assume $1/(q\delta_m) \ll 1$ together with $v/c_m \ll 1$ to uphold Eq. (3) under $\partial_t \mathbf{B} = \mathbf{0}$. We therefore define the electrostatic approximation as $\partial_t \mathbf{B} = \mathbf{0}$ and $\nabla \times \mathbf{E} = \mathbf{0}$, where the latter emerges from substituting the former into Eq. (1). Indeed, this is the approach taken by Ingebrigtsen [3]. The sufficient conditions to uphold all the Maxwell equations under the electrostatic approximation are $1/(q\delta_m) \ll 1$ and $v/c_m \ll 1$. Note that $1/(q\delta_m)$ is independent of v/c_m . For the case under interest here, the former is of the order unity while the latter is small, providing an example where $v/c_m \ll 1$ is not a *sufficient* condition to justify the electrostatic approximation.

B. Connection to the electrostatic limit

Here we remark on how our results fit into the electrostatic approximation. The electric field is then purely longitudinal, which should be screened by free charges and cannot penetrate into the conductor beyond the electrostatic screening length ($\sim \lambda_{\text{TF}}$). This apparently contradicts our results [Eq. (17)] in which the transverse component remains nonzero and unscreened up to a much larger distance $\sim q^{-1}$ even in the electrostatic limit. To resolve

this puzzle, one should carefully distinguish two possible definitions of the longitudinal and transverse components. Namely, one may call \mathbf{E}^L (\mathbf{E}^T) longitudinal (transverse) if

$$(i) \nabla \times \mathbf{E}^L = \mathbf{0} \quad (\nabla \cdot \mathbf{E}^T = 0),$$

or if

$$(ii) \nabla \cdot \mathbf{E}^L \neq 0 \quad (\nabla \times \mathbf{E}^T \neq \mathbf{0}).$$

So far, we have used (i) to classify longitudinal and transverse fields, which conforms with the terminology often used. However, (ii) is better adapted in the screening argument as it is the condition for generating the screening charges and currents through the Gauss' and Ampère-Maxwell law, respectively. The difference between the two definitions is usually immaterial, but it does matter when $\mathbf{E} = -\nabla\phi$ and $\nabla^2\phi = 0$, i.e., when ϕ is a harmonic function. Such a harmonic \mathbf{E} qualifies to be longitudinal as well as transverse under (i), whereas it is neither of them according to (ii). It turns out that \mathbf{E}^{TM} in Eq. (17) is exactly the harmonic \mathbf{E} under the electrostatic approximation. That is, \mathbf{E}^{TM} satisfies both $\nabla \cdot \mathbf{E}^{\text{TM}} = 0$ and $(\nabla \times \mathbf{E}^{\text{TM}})_y \propto iq(\alpha^2/q^2 - 1)E_z^{\text{TM}} \rightarrow 0$ as $\alpha \rightarrow q$. Thus \mathbf{E}^{TM} is longitudinal by (i) but is not by (ii). If we were to use (ii), it is reasonable to have \mathbf{E}^{TM} that penetrates deep into the conductor with a decay length of $\sim q^{-1}$. Note that abandoning the electrostatic approximation removes such ambiguity: the longitudinal and transverse components are clearly distinguished (there is no equivalent harmonic component) and they are respectively screened by induced charges and currents.

VI. QUANTITATIVE ESTIMATION

In this section, we calculate the profile of the electric current and charge density in metallic films. First, we compare the profile calculated with and without the electrostatic approximation. For this purpose, the electrical conductivity of the film is set large such that the condition for the electrostatic approximation, $1/(q\delta_m) \ll 1$, does not hold. Next, we model a system in which SAW-induced spin current was observed experimentally. Material parameters that match the experimental conditions are used. We discuss the consequence of the results obtained here on the SAW-induced spin current.

As noted in the previous section, we regard v as given and use the value of Y+128°-cut LiNbO₃, $v = 4000$ m/s [34].

In the following, we also assume $\varepsilon_r = 1$ and $q = 2\pi/10 \mu\text{m}^{-1}$. The diffusion coefficient is

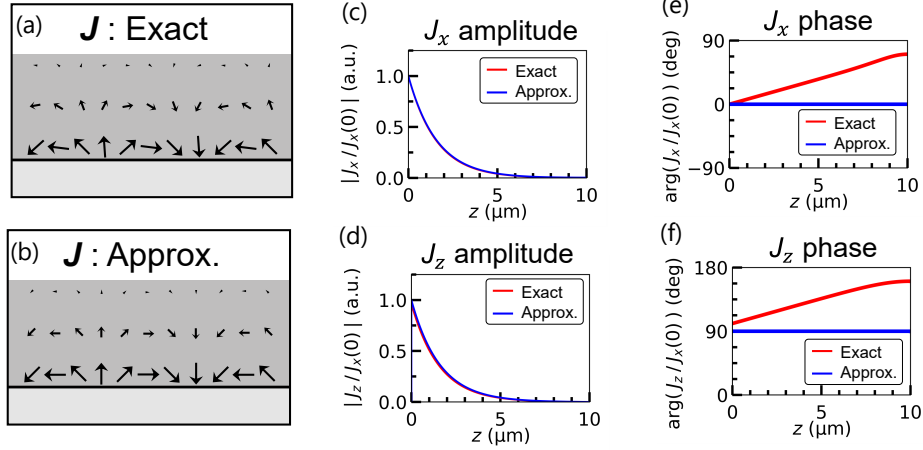


FIG. 3. (a,b) Schematic illustration of (J_x, J_z) within the metallic thick film obtained without (a) and with (b) the electrostatic approximation. The light gray region represents the piezoelectric substrate, while the dense gray region shows the metallic thin film. (c-f) Profile of the amplitude and phase of J_x (c,e) and J_z (d,f) along z -axis. The values are normalized by J_x at $z = 0$. J_x, J_z are estimated from Eq. (21) with $\sigma_c = 5 \times 10^7 / (\Omega \cdot \text{m})$, $\varepsilon_r = 1$, $d = 10 \mu\text{m}$, $v = 4000 \text{ m/s}$, and $q = 2\pi/10 \mu\text{m}^{-1}$. Note that J_y will also be induced in the presence of TE mode.

chosen to be $D_e = 3 \text{ cm}^2/\text{s}$, a representative value for metals [35, 36]. With these parameters, we obtain $\lambda_{\text{TF}} = 0.054 \text{ nm}$ and $v/c_m = 1.3 \times 10^{-5}$. The latter satisfies one of the sufficient conditions for the electrostatic approximation, $v/c_m \ll 1$.

A. Difference with the electrostatic approximation

As shown in Section III B, calculations with and without the electrostatic approximation provide quantitatively different results unless $1/(q\delta_m) \ll 1$.

To see this, we estimate the distribution of the electric current in films with large electrical conductivity: $\sigma_c = 5 \times 10^7 (\Omega \cdot \text{m})^{-1}\text{m}$. With these parameters, $q/Q \sim 10^{-5}$, $\eta \sim 10^{-10}$ and $\delta_m = 3.6 \mu\text{m}$. Consequently, we have $q\delta_m = 2.3$ that violates the condition for the electrostatic approximation.

Figure 3 shows the profiles of the electric current density profiles J_x, J_z with and without the electrostatic approximation. The solutions under the approximation are obtained by substituting $v/c_m = 0$ and $1/(q\delta_m) = 0$ into those without it. We set the film thickness $d = 10 \mu\text{m}$ to display the changes along the z -axis. Without the approximation, the electric current changes its phase monotonically along the z -axis whereas the phase remains constant

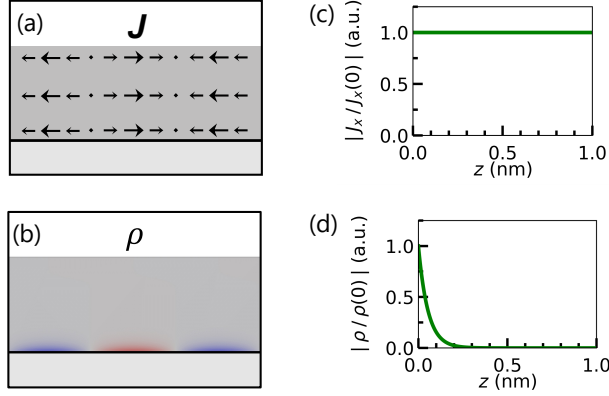


FIG. 4. (a,b) Schematic illustration of (J_x, J_z) (a), and ρ (b) within the metallic thin film. The light gray region represents the piezoelectric substrate, while the dense gray region shows the metallic thin film. J_z is almost invisible in (a) since it is several orders of magnitude smaller than J_x . (c,d) Profile of $|J_x|$ (c) and $|\rho|$ (d) along z -axis. The values are normalized at $z = 0$. J_x and ρ are estimated from Eq. (21) and Eq. (22) with $\sigma_c = 10^6 / (\Omega \cdot \text{m})$, $\varepsilon_r = 1$, $d = 1$ nm, $v = 4000$ m/s, and $q = 2\pi/10 \mu\text{m}^{-1}$. Note that J_y will also be induced in the presence of TE mode.

under the approximation This is caused by the imaginary part of α [Eq. (18)], which is not negligible for films with large conductivity. As is evident from the plots shown in Fig. 3(a,b), the phase change manifests itself in the current flow distribution along the z -axis. At a given position in the x - y plane, the current changes its direction as one moves along the z -axis when the electrostatic approximation is abandoned, whereas the direction remains the same throughout the entire film when the approximation is maintained.

B. Modeling of an experimental setup

Next, we model an experimental setup in which SAW-induced spin current was found[37]. In accordance with the experiments, the film conductivity and thickness are set to $\sigma_c = 10^6 (\Omega \cdot \text{m})^{-1}$ and $d = 1$ nm, respectively; however, qualitatively similar results are obtained as long as $d \lesssim 1/\alpha \sim 100$ nm. These parameters return $q/Q \sim 10^{-5}$, $\eta \sim 10^{-8}$ and $\delta_m = 25 \mu\text{m}$. Thus $1/(q\delta_m) \sim 0.06$, allowing one to use the electrostatic approximation. However, here we do not apply the approximation and follow the discussion described above.

From the parameters defined above, $|\alpha d| \sim qd \sim 10^{-3}$ and $Qd \sim 20$ hold so that $\sinh \alpha d \sim$

10^{-3} , $\cosh \alpha d \sim 1$, $\sinh Qd \sim \cosh Qd \gg 1$. Therefore, Eq. (34) is well approximated by

$$C_0^{\text{TM}} \sim \frac{2e^{-Qd}}{\varepsilon_r qd} \frac{E_{x0}}{\eta/qd + iq/Q}, \quad C_0^{\text{TE}} \sim E_{y0}. \quad (37)$$

Note that η cannot be set to zero even at this leading order. Using the same approximations, one obtains

$$\begin{aligned} \begin{pmatrix} E_x^{\text{TM}} \\ E_z^{\text{TM}} \end{pmatrix} &\sim \frac{\eta}{2qd} \frac{E_{x0}}{\eta/qd + iq/Q} \begin{pmatrix} e^{q(z-d)} + e^{-qz} \\ -i(e^{q(z-d)} - e^{-qz}) \end{pmatrix} \\ &\sim \frac{\eta}{qd} \frac{E_{x0}}{\eta/qd + iq/Q} \begin{pmatrix} 1 \\ i(qd/2 - qz) \end{pmatrix}, \end{aligned} \quad (38)$$

$$\begin{pmatrix} E_x^{\text{L}} \\ E_z^{\text{L}} \end{pmatrix} \sim \frac{E_{x0}e^{-Qz}}{\eta/qd + iq/Q} \begin{pmatrix} iq/Q \\ -1 \end{pmatrix}. \quad (39)$$

As shown in Eqs. (21) and (22), \mathbf{E}^{L} is effectively screened by the small factor η while \mathbf{E}^{TM} remains sizable in the film. Therefore, the charge current inside metal is completely dominated by the transverse contribution whereas the charge density is mostly induced by E_z^{L} . We note that $|E_x^{\text{TM}}| \gg |E_z^{\text{TM}}|$ is consistent with $\nabla \cdot \mathbf{E}^{\text{TM}} = 0$ as the smallness of E_z^{TM} is a result of cancellation between the C_+^{TM} and C_-^{TM} terms; such cancellation is absent in the z derivative $\partial_z E_z^{\text{TM}}$ because of the sign change of the latter term.

The uniformity of the electric current and the localization of the charge density within the metallic thin film are directly demonstrated by evaluating Eqs. (21) and (22) using Eq. (17). The results are schematically illustrated in Fig. 4 (a) and (b). Due to the small factor of η originating from the electrostatic screening, the longitudinal components of \mathbf{J} that originates from \mathbf{E}^{L} localized at the film surfaces become negligibly small. In addition, cancellation between C_+^{TM} and C_-^{TM} results in a significant decrease of J_z overall. The charge density ρ is confined at the interface between the substrate and film to screen out E_z^{L} coming from the substrate. To illustrate the distribution along z more quantitatively, the absolute values of J_x and ρ are plotted against z in Fig. 4 (c) and (d). We see that J_x is almost uniform along z in the whole film and ρ is concentrated within the range of the Thomas-Fermi length from the substrate surface.

Recent experimental work has demonstrated that SAWs induce an ac spin current in metallic thin films with significant spin-orbit interaction, an effect referred to as the acoustic spin Hall effect [37]. The observed spin current flows parallel to the surface normal with its

polarization orthogonal to both the flow and SAW propagation directions, and is distributed uniformly across the film thickness direction. Under the assumption that electric fields are efficiently screened by conduction electrons and decay rapidly in metals, the latter feature suggests that the spin current should have a mechanical origin rather than electromagnetic one. From this work, however, we conclude that the SAW-induced electric field generates an electric current uniformly in the thickness direction in metallic thin films. This allows the uniform spin current to flow in strong spin orbit metals via the spin Hall effect, which can reasonably explain the microscopic origin of the acoustic spin Hall effect.

VII. CONCLUSION

In summary, we have studied the electromagnetic response of a metallic thin film to the electric field associated with the piezoelectrically excited surface acoustic wave (SAW) without employing the electrostatic approximation. The electromagnetic field accompanying the SAW contains a component that behaves as an evanescent field and carries a transverse field, which is not screened by the electric charge but via the skin effect inside conductors. We refined the decay length of the SAW-induced electric field in conducting slabs, and found that it is determined by both the SAW wavelength and the skin depth. The electromagnetic evanescent field that accompanies SAW can therefore influence the transport properties of metallic thin films deposited on piezoelectric substrates, a playground for studies on acoustoelectronics and spintronics.

VIII. ACKNOWLEDGEMENTS

We acknowledge fruitful discussions with K. Usami. This work was partly supported by JSPS KAKENHI (Grant Nos. 20J21915, 20J20952, 21K13886, 23KJ1419, 23KJ1159, 23H05463, and 24K00576), JST PRESTO Grant No. JPMHPR20LB, Japan, and JSPS Bilateral Program Number JPJSBP120245708.

IX. APPENDIX

A. Explicit form for half-infinite piezoelectric substrate

Here we explicitly describe equations for SAWs in a piezoelectric substrate. To emphasise the algebraic structure, let us introduce three-by-three matrices

$$\begin{aligned} G_{ij} &= c_{i1j1}, & S_{ij} &= c_{i3j3}, & T_{ij} &= c_{i3j1}, \\ X_{ij} &= e_{ij1}, & Y_{ij} &= e_{ij3}. \end{aligned} \quad (40)$$

Equations (8) and (10) under the constraints Eqs. (4) and (7) can be written as

$$\begin{pmatrix} \partial_z^2 \hat{S} + iq\partial_z (\hat{T} + \hat{T}^T) - q^2 \hat{G} - \rho_p q^2 v^2 \hat{I} & -iq\hat{X}^T - \partial_z \hat{Y}^T \\ \frac{iq\hat{X} + \partial_z \hat{Y}}{\varepsilon_0} & \partial_z^2 \hat{I}_3 - iq\partial_z \hat{I}_2 + q^2 \left(\frac{\varepsilon}{\varepsilon_0} \frac{v^2}{c^2} - \hat{I}_1 \right) \end{pmatrix} \begin{pmatrix} \mathbf{u} \\ \mathbf{E} \end{pmatrix} = 0, \quad (41)$$

$$\{ \partial_z^2 Y_{3j} + iq\partial_z (X_{3j} + Y_{1j}) - q^2 X_{1j} \} u_j + (\partial_z \varepsilon_{3j} + iq\varepsilon_{1j}) E_j = 0, \quad (42)$$

where \hat{I} is the three-by-three unit matrix and

$$\hat{I}_1 = \begin{pmatrix} 0 & 0 & 0 \\ 0 & 1 & 0 \\ 0 & 0 & 1 \end{pmatrix}, \quad \hat{I}_2 = \begin{pmatrix} 1 & 0 & 0 \\ 0 & 0 & 0 \\ 0 & 0 & 1 \end{pmatrix}, \quad \hat{I}_3 = \begin{pmatrix} 1 & 0 & 0 \\ 0 & 1 & 0 \\ 0 & 0 & 0 \end{pmatrix}. \quad (43)$$

Since Eq. (41) does not contain second order derivative on E_z , the mathematical structure of the problem is harder to see than the other cases. One formal approach is to eliminate E_z and $\partial_z E_z$ by using the last of Eq. (41) and Eq. (42), which should leave an equation for \mathbf{u}, E_x, E_y of second order in ∂_z . Although this procedure cannot be used to eliminate E_z when $\varepsilon_{33} = \varepsilon_{13} = 0$, it is applicable for the Rayleigh-type SAW, the system of our interest. Then, one expects to obtain five independent solutions of the form $\propto e^{kz}$, ($k > 0$), and the stress-free boundary condition

$$\left(\partial_z \hat{S} + iq\hat{T} \right) \mathbf{u} - \hat{Y}^T \mathbf{E} = 0 \quad (44)$$

should be able to eliminate three of the five arbitrary constants, leaving two to be determined through the electromagnetic boundary conditions.

B. Surface impedance at substrate/film interface

In the main text, we expressed the electric field inside the conducting slab in terms of the electric field at the substrate/film interface. As we mentioned in the last paragraph of Sec. IV, obtaining v and the relative amplitude between E_{x0} and E_{y0} requires the continuity of H_x and D_z at $z = 0$. The conditions are equivalent to equating the surface impedance of both sides, as described by Refs. [3, 26]. The surface impedance is defined in each region independently. We first derive the analytical formula of the surface impedances in the conducting slab, which read

$$\begin{aligned} Z^{\text{TE}} &= -i\sqrt{\frac{\mu_0}{\epsilon_0}}\frac{v}{c}\frac{q}{\alpha}\frac{C_+^{\text{TE}}e^{-\alpha d} + C_-^{\text{TE}}}{C_+^{\text{TE}}e^{-\alpha d} - C_-^{\text{TE}}}, \\ Z^{\text{TM}} &= -i\sqrt{\frac{\mu_0}{\epsilon_0}}\frac{c}{\epsilon_r v}\frac{\alpha}{q}\frac{(C_+^{\text{TM}}e^{-\alpha d} - C_-^{\text{TM}}) - iq(C_+^{\text{L}}e^{-Qd} + C_-^{\text{L}})}{(C_+^{\text{TM}}e^{-\alpha d} + C_-^{\text{TM}}) - iQ(C_+^{\text{L}}e^{-Qd} - C_-^{\text{L}})}. \end{aligned} \quad (45)$$

From Eqs. (31) and (32), one obtains the surface impedance for the conducting slab as

$$Z^{\text{TE}} = i\sqrt{\frac{\mu_0}{\epsilon_0}}\frac{v}{c}\frac{q}{\alpha}\frac{q \tanh \alpha d + \alpha \gamma}{q + \alpha \gamma \tanh \alpha d}, \quad (46)$$

$$\begin{aligned} Z^{\text{TM}} &= i\sqrt{\frac{\mu_0}{\epsilon_0}}\frac{c}{v\epsilon_r(1-i\eta)}\frac{1}{q}\frac{\alpha}{q}\left[\left(\frac{q}{Q}\cosh Qd \sinh \alpha d - \frac{i\alpha\eta}{q}\sinh Qd \cosh \alpha d\right)\frac{\epsilon_r(1-i\eta)}{\gamma}\right. \\ &\quad \left. + \left(\frac{q^2}{Q^2} - \frac{\alpha^2\eta^2}{q^2}\right)\sinh Qd \sinh \alpha d + \frac{2i\alpha\eta}{Q}(1 - \cosh Qd \cosh \alpha d)\right] \\ &\quad / \left[\left\{\frac{\epsilon_r(1-i\eta)}{\gamma}\sinh Qd + \frac{q}{Q}\cosh Qd\right\}\sinh \alpha d - \frac{i\alpha\eta}{q}\sinh Qd \cosh \alpha d\right]. \end{aligned} \quad (47)$$

Z^{TM} agrees with the expression given in Ref. [3] when setting $\alpha = q$ and $\gamma = 1$. The expression of Z^{TE} can be derived only when the electrostatic approximation $v/c \rightarrow 0$ is not employed. Assuming $q\delta_m$ is neither very small nor large, Z^{TM} involves two small parameters; q/Q and η . In any case, the dominant contributions arise from the terms proportional to ϵ_r in both the numerator and denominator. We also remark that the limit $\sigma_c \rightarrow \infty$ implies $Q \rightarrow \infty, \eta \rightarrow 0$, which yields a well-defined limit and $Z^{\text{TM}} = 0$ consistent with the so-called shorted boundary condition [25].

Next we outline how the surface impedance of the adjoining piezoelectric medium can be obtained. The general structure of the bulk solution of the electromagnetic fields can be

inferred as discussed in Sec. III C. This solution should contain two arbitrary constants that characterize it (for instance, E_{x0} and E_{y0}), allowing for the numerical computation of the surface impedance Z^{TE} , Z^{TM} on the side $z < 0$ if the value of v is determined.

-
- [1] R. M. White and F. W. Voltmer, “Direct piezoelectric coupling to surface elastic waves,” *Appl. Phys. Lett.* **7**, 314 (1965).
 - [2] J. H. Collins, K. M. Lakin, C. F. Quate, and H. J. Shaw, “Amplification of Acoustic Surface Waves with Adjacent Semiconductor and Piezoelectric Crystals,” *Applied Physics Letters* **13**, 314–316 (1968).
 - [3] K. A. Ingebrigtsen, “Linear and nonlinear attenuation of acoustic surface waves in a piezoelectric coated with a semiconducting film,” *J. Appl. Phys.* **41**, 454 (1970).
 - [4] A.J. Ricco, S.J. Martin, and T.E. Zipperian, “Surface acoustic wave gas sensor based on film conductivity changes,” *Sensors and Actuators* **8**, 319–333 (1985).
 - [5] Achim Wixforth, Jörg P Kotthaus, and G Weimann, “Quantum oscillations in the surface-acoustic-wave attenuation caused by a two-dimensional electron system,” *Physical review letters* **56**, 2104 (1986).
 - [6] R. Adler, D. Janes, B. J. Hunsinger, and S. Datta, “Acoustoelectric measurement of low carrier mobilities in highly resistive films,” *Applied Physics Letters* **38**, 102–103 (1981).
 - [7] H. Fritzsche, “Analysis of the traveling-wave technique for measuring mobilities in low-conductivity semiconductors,” *Phys. Rev. B* **29**, 6672–6678 (1984).
 - [8] M. A. Paalanen, R. L. Willett, P. B. Littlewood, R. R. Ruel, K. W. West, L. N. Pfeiffer, and D. J. Bishop, “rf conductivity of a two-dimensional electron system at small landau-level filling factors,” *Phys. Rev. B* **45**, 11342–11345 (1992).
 - [9] Norbert Karl, Karl-Heinz Kraft, and Jörg Marktanner, “Charge carrier mobilities in dark-conductive organic thin films determined by the surface acoustoelectric travelling wave (saw) technique,” *Synthetic Metals* **109**, 181–188 (2000).
 - [10] C. Müller, A. A. Nateprov, G. Obermeier, M. Klemm, R. Tidecks, A. Wixforth, and S. Horn, “Surface acoustic wave investigations of the metal-to-insulator transition of V2O3 thin films on lithium niobate,” *Journal of Applied Physics* **98**, 084111 (2005).
 - [11] Mengmeng Wu, Xiao Liu, Renfei Wang, Yoon Jang Chung, Adbhut Gupta, Kirk W. Baldwin,

- Loren Pfeiffer, Xi Lin, and Yang Liu, “Probing quantum phases in ultra-high-mobility two-dimensional electron systems using surface acoustic waves,” *Phys. Rev. Lett.* **132**, 076501 (2024).
- [12] A. L. Efros and Yu. M. Galperin, “Quantization of the acoustoelectric current in a two-dimensional electron system in a strong magnetic field,” *Phys. Rev. Lett.* **64**, 1959–1962 (1990).
- [13] Vladimir I. Fal’ko, S. V. Meshkov, and S. V. Iordanskii, “Acoustoelectric drag effect in the two-dimensional electron gas at strong magnetic field,” *Phys. Rev. B* **47**, 9910–9912 (1993).
- [14] M. Rotter, A. Wixforth, W. Ruile, D. Bernklau, and H. Riechert, “Giant acoustoelectric effect in GaAs/LiNbO₃ hybrids,” *Appl. Phys. Lett.* **73**, 2128–2130 (1998).
- [15] Yawen Fang, Yang Xu, Kaifei Kang, Benyamin Davaji, Kenji Watanabe, Takashi Taniguchi, Amit Lal, Kin Fai Mak, Jie Shan, and BJ Ramshaw, “Quantum oscillations in graphene using surface acoustic wave resonators,” *Physical Review Letters* **130**, 246201 (2023).
- [16] M. Weiler, L. Dreher, C. Heeg, H. Huebl, R. Gross, M. S. Brandt, and S. T. B. Goennenwein, “Elastically driven ferromagnetic resonance in nickel thin films,” *Phys. Rev. Lett.* **106**, 117601 (2011).
- [17] L. Dreher, M. Weiler, M. Pernpeintner, H. Huebl, R. Gross, M. S. Brandt, and S. T. B. Goennenwein, “Surface acoustic wave driven ferromagnetic resonance in nickel thin films: Theory and experiment,” *Phys. Rev. B* **86**, 134415 (2012).
- [18] L. Thevenard, C. Gourdon, J. Y. Prieur, H. J. von Bardeleben, S. Vincent, L. Becerra, L. Largeau, and J. Y. Duquesne, “Surface-acoustic-wave-driven ferromagnetic resonance in (Ga,Mn)(As,P) epilayers,” *Phys. Rev. B* **90**, 094401 (2014).
- [19] R. Sasaki, Y. Nii, Y. Iguchi, and Y. Onose, “Nonreciprocal propagation of surface acoustic wave in Ni/LiNbO₃,” *Phys. Rev. B* **95**, 020407 (2017).
- [20] Mamoru Matsuo, Jun’ichi Ieda, Kazuya Harii, Eiji Saitoh, and Sadamichi Maekawa, “Mechanical generation of spin current by spin-rotation coupling,” *Phys. Rev. B* **87**, 180402 (2013).
- [21] D. Kobayashi, T. Yoshikawa, M. Matsuo, R. Iguchi, S. Maekawa, E. Saitoh, and Y. Nozaki, “Spin current generation using a surface acoustic wave generated via spin-rotation coupling,” *Phys. Rev. Lett.* **119**, 077202 (2017).
- [22] Mingxian Huang, Wenbin Hu, Huaiwu Zhang, and Feiming Bai, “Giant coupling excited by shear-horizontal surface acoustic waves,” *Phys. Rev. B* **107**, 134401 (2023).

- [23] H. F. Tiersten, “Wave propagation in an infinite piezoelectric plate,” *Journal of the Acoustical Society of America* **35**, 234 (1963).
- [24] Chin-Chong Tseng and R. M. White, “Propagation of piezoelectric and elastic surface waves on the basal plane of hexagonal piezoelectric crystals,” *J. Appl. Phys.* **38**, 4274–4280 (1967).
- [25] J. J. Campbell and W. R. Jones, “A method for estimating optimal crystal cuts and propagation directions for excitation of piezoelectric surface waves,” *IEEE Transactions on Sonics and Ultrasonics* **SU15**, 209 (1968).
- [26] K. A. Ingebrigtsen, “Surface waves in piezoelectrics,” *J. Appl. Phys.* **40**, 2681 (1969).
- [27] Konstantin Y. Bliokh, Aleksandr Y. Bekshaev, and Franco Nori, “Extraordinary momentum and spin in evanescent waves,” *Nat. Commun.* **5**, 3300 (2014).
- [28] J. L. Bleustein, “A new surface wave in piezoelectric materials,” *Appl. Phys. Lett.* **13**, 412 (1968).
- [29] Y. V. Gulyaev, “Electroacoustic surface waves in solids,” *JETP Lett.* **9**, 37 (1969).
- [30] S. F. Li, “The electromagneto-acoustic surface wave in a piezoelectric medium: The Bleustein-Gulyaev mode,” *J. Appl. Phys.* **80**, 5264 (1996).
- [31] Zhengzhi Jiang, Hongbing Cai, Robert Cernansky, Xiaogang Liu, and Weibo Gao, “Quantum sensing of radio-frequency signal with NV centers in SiC,” *Sci. Adv.* **9**, eadg2080 (2023).
- [32] Cecile Skoryna Kline, Jorge Monroy-Ruz, and Krishna C Balram, “Piezoelectric microresonators for sensitive spin detection,” *arXiv:2405.02212* (2024).
- [33] K. A. Ingebrigtsen and A. Tønning, “Elastic surface waves in crystals,” *Physical Review* **184**, 942–951 (1969).
- [34] S. Datta, *Surface Acoustic Wave Devices* (Prentice-Hall, 1986).
- [35] Sadamichi Maekawa, Sergio O. Valenzuela, Eiji Saitoh, and Takashi Kimura, *Spin Current* (Oxford University Press, 2017).
- [36] Yasuhiro Niimi, Dahai Wei, Hiroshi Idzuchi, Taro Wakamura, Takeo Kato, and YoshiChika Otani, “Experimental verification of comparability between spin-orbit and spin-diffusion lengths,” *Phys. Rev. Lett.* **110**, 016805 (2013).
- [37] T. Kawada, M. Kawaguchi, T. Funato, H. Kohno, and M. Hayashi, “Acoustic spin Hall effect in strong spin-orbit metals,” *Science Advances* **7**, eabd9697 (2021).